Structural insight on the mechanism of an electron-bifurcating [FeFe] hydrogenase

James Birrell (james.birrell@cec.mpg.de)
Max Planck Institute for Chemical Energy Conversion https://orcid.org/0000-0002-0939-0573
Chris Furlan
University of York
Nipa Chongdar
Max Planck Institute for Chemical Energy Conversion
Pooja Gupta
University of York
Wolfgang Lubitz
Max Planck Institute for Chemical Energy Conversion https://orcid.org/0000-0001-7059-5327
Hideaki Ogata
Nara Institute of Science and Technology https://orcid.org/0000-0002-2894-2417
James Blaza
University of Cambridge https://orcid.org/0000-0001-5420-2116

Article

Keywords:

Posted Date: December 3rd, 2021

DOI: https://doi.org/10.21203/rs.3.rs-1116484/v1

Abstract

Electron-bifurcation is a fundamental energy conservation mechanism in nature. The electron-bifurcating [FeFe] hydrogenase from *Thermotoga maritima* (HydABC) requires both NADH and ferredoxin to reduce protons generating hydrogen. The mechanism of electron-bifurcation in HydABC remains enigmatic primarily due to the lack of structural information. Here, we present a 2.3 Å electron cryo-microscopy structure of HydABC. The structure is a heterododecamer composed of two independent 'halves' each made of two strongly interacting HydABC heterotrimers electrically connected via a [4Fe-4S] cluster. A central electron transfer pathway connects the active sites for NADH oxidation and proton reduction. Symmetry expansion identified two conformations of a flexible iron-sulfur cluster domain: a "closed bridge" and an "open bridge" conformation, where a Zn^{2+} site may act as a "hinge" allowing domain movement. Based on these structural revelations, we propose two new mechanisms of electron-bifurcation in HydABC.

Introduction

Electron bifurcation splits a pair of electrons from a single two-electron donor to two different spatially separated electron acceptors with one being at a lower redox potential than the donor (*1*). This process drives thermodynamically unfavourable (endergonic) redox reactions by directly coupling them to energetically favourable (exergonic) redox reactions and, hence, it represents an alternative energy coupling mechanism to the well-known chemiosmotic coupling principle (*2*). Enzymes using electron-bifurcating are found in numerous biochemical pathways including respiration, photosynthesis, methanogenesis and the Wood-Ljundahl pathway of acetogensis (*3*– *5*). The process of electron bifurcation represents an exquisite example of how biochemical systems can use thermodynamic driving forces in a flexible and efficient manner and bifurcating enzymes hold potential as 'molecular transformers' in synthetic biology applications.

Electron bifurcation was first described in the Q-cycle of the respiratory complex III where the two electrons originating from the oxidation of ubiquinol are bifurcated via a high potential pathway to cytochrome c, and via a low potential pathway to reduce ubiquinone to ubiquinol (*6*, *7*). This process has recently been discovered in a number of other enzymes where an exergonic electron transfer process is used to drive an endergonic one (*3*– *5*). Many of these enzymes have been proposed to utilize flavin-based electron bifurcation (FBEB), in which a flavin mononucleotide (FMN) or flavin adenine dinucleotide (FAD) cofactor serves as the branch point for electrons. It first accepts a hydride from an intermediate potential redox couple (typically NAD(P)H) and then sends one electron down a high potential pathway, generating an unstable, low potential semi-reduced FMN, with low enough reducing power to send the second electron down a low potential pathway. The importance of FBEB in microbial metabolism and energy conservation is well acknowledged, but its mechanism is still poorly understood, with only a few examples so far being studied in detail, such as butyryl-CoA dehydrogenase-electron-transferring flavoprotein complex (Bcd-EtfAB) and Fd-dependent transhydrogenase (NfnI) (*8*).

The heterotrimeric [FeFe] hydrogenase, HydABC, from *Thermotoga maritima* is a soluble cytoplasmic enzyme involved in fermentation, which accepts electrons from the one-electron carrier ferredoxin (E_m = -453 mV at 80 °C, (*9*)), which is reduced during pyruvate metabolism, and the two-electron carrier NADH (E_m = -320 mV at pH 7, (*9*)), produced during glucose metabolism, to reduce protons to hydrogen ($E^{\circ\prime}$ = -420 mV at pH 7, (*9*)). The mechanism by which this enzyme functions is debated, however, the predominant view is that an FBEB mechanism is operative (*10*). The biochemically characterized FMN at the NADH binding site is unlikely to act as a bifurcating center for the following reasoning. As mentioned above a bifurcation centre should accept two electrons from at intermediate potential and donate one at high potential and the second at low potential. Since the FMN accepts electrons from H_2 (intermediate potential) and directly donates a hydride to NAD^+ (high potential), there is no way for the FMN to donate a second electron to ferredoxin.

Therefore, the site of bifurcation has been speculated to be a second flavin cofactor (*11*). However, biochemical studies do not corroborate the presence of the second flavin (*12*). In another hypothesis, the hydrogen conversion center, the so-called H-cluster, which also undergoes two-electron redox chemistry, is speculated to be the electron-bifurcation center (*7*). However, spectroscopic studies suggest that the H-cluster of HydABC has similar redox properties to the non-bifurcating [FeFe] hydrogenases, having a stable one-electron reduced state, and is, therefore, also unlikely to be the site of bifurcation (*12*).

As structural data would reveal the complex arrangement of redox cofactors in this enzyme and provide a stronger basis for understanding the mechanism of electron bifurcation, here we report a 2.3 Å resolution structure of HydABC based on electron cryo-microscopy (cryo-EM) of single particles. The cryo-EM structure suggests a synergic coupling between two HydABC heterotrimers connected through the His-ligated [4Fe-4S] cluster in the HydA subunit, which may allow functionally important electron exchange between the two heterotrimers. The structure also reveals flexible C-terminal (CT) domains in HydA and HydB (here named “bridge” domains), which contain additional iron-sulfur clusters. These domains interact through non-covalent interactions and may provide a second electron transfer pathway. Thus, this structure provides details of the arrangement of the redox clusters in HydABC, based on which two novel mechanisms of electron-bifurcation are proposed.

Results

The structure of HydABC

The heterologous production of apo-HydABC in *Escherichia coli* was described recently (12). Here, we have used this heterologously expressed HydABC to prepare the cryo-EM grids. Following the grid imaging, data collection, and processing, we obtained a 2.3 Å resolution map when D2 symmetry was enforced (fig. S1, fig. S2, A). Into this, an atomic model of HydABC was constructed, starting with a homology model based on homologous subunits in bacterial complex I (12, 13), together with *ab initio* model building in regions of the highest resolution. Initially, the last 91 and 61 C-terminal (CT) residues of

HydA and HydB, respectively, could not be built as they were not present in the homology model and had a low resolution in the map, indicating regions of high heterogeneity (explored later).

The processed cryo-EM map shows that the heterotrimeric HydABC forms a tetrameric complex, $Hyd(ABC)_4$ of HydABC heterotrimer units (protomers). Oligomerization of HydABC occurs through interactions between four HydA subunits in the core of the complex (Fig. 1, A see also Movie S1). Each HydA has extensive interactions with one adjacent HydA chain (buried surface area of 2,280 $Å^2$), and minor interactions with another HydA chain (780 $Å^2$) (Fig. 1, A). HydB is tightly bound to a single HydA (buried surface area of 1,232 $Å^2$, table S1) but with minor interactions between HydB of one heterotrimer and HydA and HydB in another heterotrimer. HydB and HydC extend outward from the core and form the four lobes clearly visible in the 2D class averages (fig. S3). The HydA core is the best resolved part of the map, consistent with the core being rigid and homogenous (fig. S4).

Based on the density map, each HydABC protomer appears to contain nine redox cofactors including five [4Fe-4S] clusters (one of which forms the [4Fe-4S] subcluster of the H-cluster), three [2Fe-2S] clusters, and one FMN. However, based on published Fe quantitation as well as published sequence analysis predictions we expect a total of seven [4Fe-4S] clusters (including the subcluster of the H-cluster) and four [2Fe-2S] clusters in each HydABC protomer (14, 15). According to sequence predictions, these missing clusters should be located in the less well resolved CT regions of the HydA and HydB subunits (discussed below) (14). Interestingly, a high-density site, likely a monometallic center, is found in the resolvable part of the HydB-CT domain. Inductively-coupled plasma mass spectrometry on the separately produced and purified HydB subunit identified 0.99 ± 0.43 Zn/protein and ≈14.2 ± 1.5 Fe/protein. As the observed Fe-content matches with the estimated Fe-content of HydB, which is expected to contain three [4Fe-4S] clusters and one [2Fe-2S] cluster (14 Fe/protein), these results allow us to assign the metal center as zinc (Zn^{2+}). This is further supported by the identities of the ligating residues: three cysteines and one histidine in a tetrahedral coordination geometry (fig. S5, C) (16).

Cofactor arrangement in HydABC

Electron transfer chains, often connecting distant active sites, are composed of redox-active cofactors usually less than 14 Å apart to allow sufficiently fast electron tunnelling through the protein dielectric to sustain catalysis (17). In each HydABC heterotrimer, the spatially distant H-clusters and FMN centers are electrically connected via a chain of four FeS clusters (A1, A2, A3, and B2, see Fig. 1, D for cluster nomenclature). The edge-to-edge distances between all these clusters are < 15 Å and within a distance for electron transfer at physiologically relevant rates (Fig. 1, D). Among the three remaining FeS clusters, the [4Fe-4S] cluster from HydA (A4) lies at the interface of the two tightly interacting HydA chains, and the two [2Fe-2S] clusters from HydC (C1) and HydB (B1) subunits lie in the vicinity, but on the opposite side, of the FMN toward a dangling helix at the N-terminus of HydB (fig. S6). This helix has locally lower resolution indicating some structural heterogeneity. Similar structural features have been suggested to function as a “fishing rod” for catching ferredoxin in a “fly casting” mechanism in cyanobacterial complex I (18) and ferredoxin $NADP^+$ reductase (19, 20). Furthermore, a formate dehydrogenase enzyme

that is closely related to HydABC but which does not bind ferredoxin, is specifically missing this helix (21). Thus, we suggest that the N-terminus of HydB may be the region where ferredoxin binds and transfers electrons to the B1 cluster. Electrons from ferredoxin would then be transferred from B1 to C1, and possibly to the FMN. However, the distance between C1 and FMN is ~16 Å, which is at the theoretical limit for fast electron transfer (17).

Within the $Hyd(ABC)_4$ complex, there appear to be two redox networks, each composed of two electrically connected HydABC protomers, separated by at least 50 Å and held together by extensive HydA-HydA interactions (Fig. 1, B and C). The large distance between each network indicates there is no possibility for electrons to be exchanged and that they probably function independently (Fig. 1, C). The two tightly interacting HydABC protomers within the $Hyd(ABC)_2$ unit are electrically connected through the His-ligated [4Fe-4S] cluster (A4) in HydA (Fig. 1, B), part of the so-called Y-junction of iron-sulfur clusters (22). This junction is well conserved in a wide number of structurally related enzymes, but its function is unknown. In HydABC it is clear that the Y-junction connects the NADH and ferredoxin oxidation sites to the hydrogenase active site and to the neighboring protomer. The two A4 clusters are separated by 9.0 Å and have the possibility to allow overflow of electrons from one protomer to the other. An electrical connection between two identical protomers has already been observed in cytochrome bc_1 (23), called an electronic 'bus-bar', which is speculated to have a number of possible roles such as allowing the physiological function of the protein even after operational damage of one of the two protomers.

Structural comparison of HydABC with homologous proteins

The spatial arrangement of subunits HydA, B and C in the HydABC protomer is similar to that of subunits Nqo3, Nqo1, and Nqo2, respectively, in the NADH-oxidation (N) module of *Thermus thermophilus (Tt)* respiratory complex I (fig. S7). This comparison is useful because complex I is structurally well-characterised, but does not oxidize ferredoxin or carry out electron-bifurcation. Therefore, structural differences between the subunits of complex I an HydABC may reveal important insight into the mechanism of electron transfer in the latter. The individual subunits are structurally highly similiar, with the highest similarity between HydB and Nqo1 (rmsd 1.040 Å) (24), followed by HydC and Nqo2 (rmsd 1.152 Å) and the lowest similarity between HydA and Nqo3 (rmsd 1.294 Å) (Fig. 2, A). The remarkable structural similarities between HydB and Nqo1 subunits agree with their common evolutionary origins (25), and suggest that NADH oxidation follows a similar mechanism in both enzymes (Fig. 2, B). The structural differences between Nqo3 and HydA likely reflect the fact that the latter accommodates the hydrogenase H-cluster and facilitates oligomerization of the $Hyd(ABC)_4$ complex.

The structural similarities between HydABC and *Tt* respiratory complex I are also reflected by the FeS clusters positioning that is in excellent agreement in these two proteins (Fig. 2, C). However, in contrast to the *Tt* complex I, the HydABC protomers contain five additional FeS clusters. One of these additional clusters is a [4Fe-4S] cluster (A3) that electrically connects the [4Fe-4S] subcluster of the H-cluster

(analogous to the cluster N7 in *Tt* complex I) with the rest of the electron transfer network. Another additional cluster is a [2Fe-2S] cofactor in HydB (B1) that is electrically connected to the [2Fe-2S] cluster in HydC (C1, analogous to N1a in *Tt* complex I); due to this connection and the proximity of HydC to the "bridge" domains (discussed later) it is likely that the [2Fe-2S] cluster in HydC has an important role in the mechanism of electron bifurcation, this is in contrast to its analogous N1a cluster in complex I, the role of which is unclear but is certainly not part of the main catalytic electron transport pathway (26, 27).

The HydA subunit has close structural homology (35% sequence identity) to the well-characterized monomeric non-bifurcating [FeFe] hydrogenase from *Clostridium pasteurianum*, *Cp*I. In contrast to electron bifurcating [FeFe] hydrogenases, non-bifurcating [FeFe] hydrogenases use a single redox partner, typically ferredoxin. Aligning the two enzymes shows high similarity (rmsd 1.119 Å) and excellent conservation of the FeS clusters, including the A4 cluster, which connects neighboring HydA subunits in HydABC (Fig. 3). However, in *Cp*I, for which ferredoxin is the only redox partner, the cluster homologous to A4 is thought to lead to the ferredoxin binding site (28). The multimerization of HydA blocks this site, so the two enzymes must have different ferredoxin binding sites. This re-arrangement is an example of how closely related systems may have different electron-transfer pathways formed by different multimerization of their subunits.

A bridging domain formed by the flexible C-termini of the HydA and HydB subunits

The core of the tetrameric HydABC complex is very well resolved, reaching a local resolution of 2.2 Å. However, the lobes formed from HydA and HydB subunits have substantially lower local resolution (~3 Å), due to increased heterogeneity (fig. S4) and low intensity, blurred map density was observed between the lobes of electrically connected HydABC protomers (fig. S8, A). To investigate the blurred regions, symmetry expansion followed by classification was explored to separate the different conformations into classes. Initial attempts to use D2 symmetry, to match the core, resulted in maps no better than before, however, using C2 symmetry revealed two classes with bridging density between the HydB lobes (Fig. 4, A) with local resolution similar to the lobes formed from HydA and HydB (Fig. 4, B). This bridging density breaks the rotational symmetry between the protomers in the $Hyd(ABC)_2$ unit, explaining why D2 symmetry expansion was ineffective. The two classes correspond to the bridge domain being formed between different HydB lobes: when rotated by 180°, the bridges are identical (Fig. 4, A and C). Despite extensive attempts, we were unable to find a class with both bridges in the closed conformation. The observation that both bridges cannot close simultaneously suggests that these behave as reciprocating elements. A similar observation was made for the Rieske domains in the bifurcating bc_1 complex (30).

To further explore the particles without a bridge a further classification was used (Fig. S8, B). It was possible to obtain a low-resolution map of a class where the HydB CT domain was found in an 'open' conformation (Fig. 4, D). The movement of the HydB C-terminal domain between the bridge-open and bridge-closed classes is shown in Fig. 4, E and Movie S2.

In the bridge-containing structure, the two C-terminal [4Fe-4S] clusters (named B3 and B4, Fig. 4, F) of HydB are close enough to exchange electrons with each other but are too far from the next nearest FeS clusters, such as cluster C1 (≈ 35 Å away) or cluster A5 (≈ 32 Å away). Furthermore, cluster A5 is completely electrically isolated with all the nearest clusters being >30 Å away. Thus, unless the HydA and HydB bridge domains undergo substantial conformational changes, the FeS clusters A5, B3 and B4 cannot participate in electronic exchange with the rest of the enzyme.

The bridge structure is particularly interesting as it appears that the C-terminal cysteine residues of HydB responsible for coordinating [4Fe-4S] clusters in the bridge are conserved in all biochemically characterized electron-bifurcating [FeFe] hydrogenases (31, 32). However, they all lack the analogous part of the bridge domain in HydA, which contains the A5 cluster.

Discussion

HydABC is not a typical flavin based electron bifurcating enzymesas it lacks a flavin center capable of accepting two electrons from an intermediate potential redox couple i.e. $2H^+/H_2$ (-410 mV at pH 7) and splitting them so that one electron goes toward a high potential couple i.e. NAD^+/NADH (-320 mV at pH 7), and the other goes toward a low potential couple i.e. ferredoxin (-450 mV). The hypothesis that a second flavin site i responsible for bifurcation (11) is neither supported by the biochemical experiments (12), nor by the cryoEM structure of HydABC presented herein: a single flavin (the FMN in HydB) that accepts a hydride from NADH, exists in this enzyme. The second hypothesis, that the H-cluster is the bifurcation center (7), is not supported by the fact that the H-cluster of HydABC shows similar behaviour to the H-cluster from non-bifurcating [FeFe] hydrogenases (12). Structural comparison of the HydA subunit (of HydABC) with the non-bifurcating [FeFe] hydrogenase CpI also reveals that the primary and secondary coordination spheres of the H-cluster are highly conserved in the two enzymes, thereby, supporting our previous conclusion (12).

Having excluded the H-cluster and FMN, we propose that the bifurcation site is an iron-sulfur cluster or a group of iron-sulfur clusters and are now able to provide two potential mechanisms, both involving the HydB-CT domain. This domain, carrying the B3 and B4 clusters, is found in all characterized electron-bifurcating [FeFe] hydrogenases but is absent in non-bifurcating NAD^+-dependent multimeric [FeFe] hydrogenases (31, 32). Therefore, these clusters are considered an essential component of the mechanism. In Mechanism 1 (Fig. 5A), H_2 is oxidized by the H-cluster and electrons are sent down the core electron transfer pathway to the FMN. Meanwhile electrons in the adjacent protomer are picked up by cluster A´5, through a large scale conformational change and transferred to the B3/B4 clusters in the bridge. Another conformational change moves the B3/B4 clusters close to the B1/C1 clusters for electron transfer to ferredoxin while NAD^+ is reduced to NADH at the FMN. In Mechanism 2 (Fig. 5B), electrons from H_2 oxidation at the H-cluster travel via the core electron transfer pathway to FMN/C1 and then to the B3/B4 clusters in the bridge causing the bridge to close. This then allows a second H_2 oxidation to reduce

the FMN. NAD^+ reduction triggers the bridge to reopen moving the reduced B3/B4 clusters close to the B1/C1 pair allowing electron transfer to ferredoxin.

In summary, our cryo-EM structure reveals essential information on the arrangement of cofactors and active sites within *T. maritima* HydABC, including inter-protomer electronic wiring. Using symmetry expansion, we have also observed two conformations of the HydB-CT domain, a domain that is unique to and conserved in bifurcating hydrogenases, consistent with mechanistically relevant conformational changes. These structural revelations open up new avenues for mechanistic views on electron-bifurcation wherein sophisticated arrangements of FeS clusters could act as the bifurcation-center. Such mechanisms may also be operative in other enzymes homologous to HydABC. By resolving these crucial structural details, the mechanism of bifurcation can now be tackled using site directed mutagenesis coupled to kinetic and spectroscopic studies.

Online Methods

Protein expression and purification

HydABC and HydB were produced heterologously in *Escherichia coli* BL21(DE3) *ΔiscR* cells under anaerobic growth conditions and purified in an anaerobic glovebox (Coy, 2% H_2 in N_2) using Streptactin (IBA) affinity chromatography and size exclusion chromatography (GE Healthcare) as previously described (12). For these studies, we did not incorporate the $[2Fe]_H$ subcluster to form the holo-enzyme. Previous studies with the *Cp*I [FeFe] hydrogenase showed essentially no difference in the protein structure between the apo-hydrogenase lacking the $[2Fe]_H$ subcluster (29) Sample purity and quality were checked by SDS-PAGE and UV-vis spectrophotometry. Samples in 10 mM Tris-HCl, 150 mM NaCl, pH 8 were frozen at -80°C until further use.

Inductively-coupled plasma mass spectrometry (ICP-MS)

For ICP-MS, a sample of the HydB subunit, buffer exchanged into 10 mM MOPS pH 7 and concentrated to 621 µM, and a sample of 10 mM MOPS pH 7 were measured by Mikroanalytisches Laboratorium Kolbe (www.mikro-lab.de). The samples were digested using a CEM Model MARS6 microwave digestion unit and measured on an Agilent Model 7900 ICP-MS.

Grid preparation and imaging

1.2/1.3 UltrAuFoil grids were glow discharged (PELCO easiGlow) for 90 s on each side using atmospheric gas before mounting in Vitrobot (model IV) tweezers (Thermo Fisher Scientific). Individual HydABC aliquots were defrosted and 2.5 µL immediately placed onto the grid, blotted, and plunged into liquid ethane. 12 grids were prepared, varying blot time from 2 - 4 s with 0.75-1.5 mg mL^{-1} protein; blot force was constant at -5. Following screening, a grid at 1 mg mL^{-1} protein concentration was selected for data collection on a Titan Krios microscope operated at 300 kV with a K2 detector and energy filter. The energy filter was set to a 20 eV window. 3 exposures were collected per hole, and the autofocus routine was run

every 10 µm. AutoCTF was used to correct for astigmatism and coma. 4790 movies of 48 frames each were collected. The total fluence was 57 electrons / $Å^2$.

Image processing

The Relion pipeline was used for all image processing. Whole micrograph motion correction and damage weighting was performed using the implementation of MotionCor2 in Relion (33). Initial CTF values were determined with CTFFIND4 (34) and particles were picked using a low resolution (≈10 Å) preliminary dataset that was previously collected (not described here). The early stages of 2D and 3D classification used images with the original pixel size downsampled from 0.85 Å to 3.4 Å/pixel. The particles were cleaned using two rounds of reference-free 2D classification. An initial model was generated in Relion and coarse 3D classification (7.5° sampling) without symmetry being enforced was used to remove broken particles. The particles were re-extracted with the original pixel size of 0.85 Å/pixel and 3D auto-refinement of these particles resulted in a 2.5 Å resolution structure when D2 symmetry was applied and after iterative CTF refinement of anisotropic magnification, trefoil and 4th order aberrations; astigmatism and defocus were fitted on a per-particle basis. The map displayed the features expected at such a resolution, with rotamers of many side chains being clear and water molecules being visible in well-resolved regions. The Bayesian polishing function of Relion-3.1 (35) resulted in a 2.3 Å resolution structure when D2 symmetry was applied (fig. S1); further CTF refinement led to no further gains in resolution. The final calibrated pixel size was 0.824 Å.

The HydA and HydB CT domains forming the “bridge” between lobes were found using the symmetry expansion tools in Relion. The high-resolution D2 refinement was used as a starting point. The relion_symmetry_expand command was used to apply a C2 symmetry operator to the particles in the refined .star file. A 20 Å low-pass filtered mask, generated from fitted atomic coordinates and expanded by 20 pixels with 6 pixels soft-edge, was then applied to half of the complex containing two tightly connected HydABC protomers with a complete electron transfer network. A mask was then created that included exclusively the two “bridges” densities in the $Hyd(ABC)_2$ unit (20 Å low-pass filter, 6 pixels soft edge), allowing a better 3D classification without losing any signal in the “bridges”. The resulting “bridged” classes (bridge backward and forward) were refined with C1 symmetry applying a 6 pixel soft edge mask that included the $Hyd(ABC)_2$ unit with two bridges, reaching a resolution of 2.8 Å for both the classes.

To explore the location of the HydB in the non-bridged class, a mask was created around the suspected area and used for classification and refinement (fig. S8, B). The improved map allowed an improved mask to be created for a final round of classification and refinement. The resulting map density is of insufficient quality for *ab initio* model building, but the strong FeS signals allowed the HydB CT-domain to be docked in place (Fig. 4, D).

Model building and validation

We used a homology model generated based on bacterial complex I (13) discussed in our recent paper on HydABC (12) as a starting point for model building. Here the Nqo3 subunit of complex I is related to HydA, Nqo1 to HydB, and Nqo2 to HydC. The map density was sufficiently strong to allow ab initio building of the non-conserved regions of HydA and HydB in the well-resolved parts of the D2 map, however without further classification many parts of HydB and HydC were poorly resolved. Model refinement was performed using Phenix real-space refinement. Phenix now automatically recognises the ligation between FeS clusters and cysteines, so it is no longer necessary to manually define these restraints or to provide the correct definition of the FeS geometry (36).

The “bridge” is formed from 91 residues of the CT of HydA and 61 residues of the CT of HydB. The HydA CT “bridge” domain has homology with the CT of HndA from the NADP-reducing hydrogenase complex in *Desulfovibrio fructosovorans* (37) and 82 CT residues of *T. maritima* HydC. The HydB CT “bridge” domain has homology with bacterial 2x[4Fe-4S] ferredoxin domains. In both cases, Phyre2 was used to build a homology model from this information, which was further built into the density, combined with the model for the rest of the complex built from the D2 map and refined (38).

References

1. C. E. Wise, A. E. Ledinina, J. L. Yuly, J. H. Artz, C. E. Lubner, The role of thermodynamic features on the functional activity of electron bifurcating enzymes. *Biochim. Biophys. Acta - Bioenerg.* **1862**, 148377 (2021).
2. P. Rich, The cost of living. *Nature.* **421**, 583 (2003).
3. J. W. Peters, A. F. Miller, A. K. Jones, P. W. King, M. W. W. Adams, Electron bifurcation. *Curr. Opin. Chem. Biol.* **31**, 146–152 (2016).
4. V. Müller, N. P. Chowdhury, M. Basen, Electron bifurcation: a long-hidden energy-coupling mechanism. *Annu. Rev. Microbiol.* **72**, 331–353 (2018).
5. A. M. G. Costas, S. Poudel, A. F. Miller, G. J. Schut, R. N. Ledbetter, K. R. Fixen, L. C. Seefeldt, M. W. W. Adams, C. S. Harwood, E. S. Boyd, J. W. Peters, Defining electron bifurcation in the electron-transferring flavoprotein family. *J. Bacteriol.* **199**, e00440-17 (2017).
6. E. Darrouzet, C. C. Moser, P. L. Dutton, F. Daldal, Large scale domain movement in cytochrome bc1: A new device for electron transfer in proteins. *Trends Biochem. Sci.* **26**, 445–451 (2001).
7. J. W. Peters, D. N. Beratan, G. J. Schut, M. W. W. Adams, On the nature of organic and inorganic centers that bifurcate electrons, coupling exergonic and endergonic oxidation-reduction reactions. *Chem. Commun.* **54**, 4091–4099 (2018).
8. W. Buckel, R. K. Thauer, Flavin-based electron bifurcation, a new mechanism of biological energy coupling. *Chem. Rev.* **118**, 3862–3886 (2018).
9. G. J. Schut, M. W. W. Adams, The iron-hydrogenase of *Thermotoga maritima* utilizes ferredoxin and NADH synergistically: A new perspective on anaerobic hydrogen production. *J. Bacteriol.* **191**, 4451–4457 (2009).

10. W. Buckel, R. K. Thauer, Flavin-based electron bifurcation, ferredoxin, flavodoxin, and anaerobic respiration with protons (Ech) or NAD^+ (Rnf) as electron acceptors: a historical review. *Front. Microbiol.* **9**, 401 (2018).
11. W. Buckel, R. K. Thauer, Energy conservation via electron bifurcating ferredoxin reduction and proton/Na^+ translocating ferredoxin oxidation. *Biochim. Biophys. Acta - Bioenerg.* **1827**, 94–113 (2013).
12. N. Chongdar, K. Pawlak, O. Rüdiger, E. J. Reijerse, P. Rodríguez-Maciá, W. Lubitz, J. A. Birrell, H. Ogata, Spectroscopic and biochemical insight into an electron-bifurcating [FeFe] hydrogenase. *J. Biol. Inorg. Chem.* **25**, 135–149 (2020).
13. R. Baradaran, J. M. Berrisford, G. S. Minhas, L. A. Sazanov, Crystal structure of the entire respiratory complex I. *Nature.* **494**, 443–448 (2013).
14. M. F. J. M. Verhagen, T. O'Rourke, M. W. W. Adams, The hyperthermophilic bacterium, Thermotoga maritima, contains an unusually complex iron-hydrogenase: amino acid sequence analyses versus biochemical characterization. *Biochim. Biophys. Acta - Bioenerg.* **1412**, 212–229 (1999).
15. M. F. J. M. Verhagen, T. W. O'Rourke, A. L. Menon, M. W. W. Adams, Fe-only hydrogenase from *Thermotoga maritima*. *Methods Enzymol.* **331**, 216–226 (2001).
16. S. M. Ireland, A. C. R. Martin, ZincBind - The database of zinc binding sites. *Database*. 2019, baz006 (2019).
17. C. C. Page, C. C. Moser, X. Chen, P. L. Dutton, Natural engineering principles of electron tunnelling in biological oxidation-reduction. *Nature.* **402**, 47–52 (1999).
18. J. M. Schuller, J. A. Birrell, H. Tanaka, T. Konuma, H. Wulfhorst, N. Cox, S. K. Schuller, J. Thiemann, W. Lubitz, P. Sétif, T. Ikegami, B. D. Engel, G. Kurisu, M. M. Nowaczyk, Structural adaptations of photosynthetic complex I enable ferredoxin-dependent electron transfer. *Science* **363**, 257–260 (2019).
19. M. Maeda, Y. H. Lee, T. Ikegami, K. Tamura, M. Hoshino, T. Yamazaki, M. Nakayama, T. Hase, Y. Goto, Identification of the N- and C-terminal substrate binding segments of ferredoxin-$NADP^+$ reductase by NMR. *Biochemistry.* **44**, 10644–10653 (2005).
20. N. Cassan, B. Lagoutte, P. Sétif, Ferredoxin-$NADP^+$ reductase: Kinetics of electron transfer, transient intermediates, and catalytic activities studied by flash-absorption spectroscopy with isolated photosystem I and ferredoxin. *J. Biol. Chem.* **280**, 25960–25972 (2005).
21. C. Radon, G. Mittelstädt, B. R. Duffus, J. Bürger, T. Hartmann, T. Mielke, C. Teutloff, S. Leimkühler, P. Wendler, Cryo-EM structures reveal intricate Fe-S cluster arrangement and charging in Rhodobacter capsulatus formate dehydrogenase. *Nat. Commun.* **11**, 1–9 (2020).
22. K. Zuchan, F. Baymann, C. Baffert, M. Brugna, W. Nitschke, The dyad of the Y-junction- and a flavin module unites diverse redox enzymes. *Biochim. Biophys. Acta - Bioenerg.* **1862**, 148401 (2021).
23. M. Świerczek, E. Cieluch, M. Sarewicz, A. Borek, C. C. Moser, P. L. Dutton, A. Osyczka, An electronic bus bar lies in the core of cytochrome bc_1. *Science* **329**, 451–454 (2010).

24. J. Gutiérrez-Fernández, K. Kaszuba, G. S. Minhas, R. Baradaran, M. Tambalo, D. T. Gallagher, L. A. Sazanov, Key role of quinone in the mechanism of respiratory complex I. *Nat. Commun.* **11**, 4135 (2020).
25. G. J. Schut, E. S. Boyd, J. W. Peters, M. W. W. Adams, The modular respiratory complexes involved in hydrogen and sulfur metabolism by heterotrophic hyperthermophilic archaea and their evolutionary implications. *FEMS Microbiol. Rev.* **37**, 182–203 (2013).
26. J. A. Birrell, K. Morina, H. R. Bridges, T. Friedrich, J. Hirst, Investigating the function of [2Fe-2S] cluster N1a, the off-pathway cluster in complex I, by manipulating its reduction potential. *Biochem. J.* **456**, 139–146 (2013).
27. E. Gnandt, J. Schimpf, C. Harter, J. Hoeser, T. Friedrich, Reduction of the off-pathway iron-sulphur cluster N1a of *Escherichia coli* respiratory complex I restrains NAD^+ dissociation. *Sci. Rep.* **7**, 8754 (2017).
28. J. H. Artz, D. W. Mulder, M. W. Ratzloff, C. E. Lubner, O. A. Zadvornyy, A. X. Levan, S. G. Williams, M. W. W. Adams, A. K. Jones, P. W. King, J. W. Peters, Reduction potentials of [FeFe]-hydrogenase accessory iron-sulfur clusters provide insights into the energetics of proton reduction catalysis. *J. Am. Chem. Soc.* **139**, 9544–9550 (2017).
29. J. Esselborn, N. Muraki, K. Klein, V. Engelbrecht, N. Metzler-Nolte, U. P. Apfel, E. Hofmann, G. Kurisu, T. Happe, A structural view of synthetic cofactor integration into [FeFe]-hydrogenases. *Chem. Sci.* **7**, 959–968 (2016).
30. M. Maldonado, F. Guo, J. A. Letts, A. P. Carter, Atomic structures of respiratory complex III_2, complex IV, and supercomplex III_2-IV from vascular plants. *Elife.* **10**, 1–34 (2021).
31. N. A. Losey, F. Mus, J. W. Peters, H. M. Le, M. J. McInerney, *Syntrophomonas wolfei* uses an NADH-dependent, ferredoxinindependent [FeFe]-hydrogenase to reoxidize NADH. *Appl. Environ. Microbiol.* **83**, e01335-17 (2017).
32. N. A. Losey, S. Poudel, E. S. Boyd, M. J. McInerney, The beta subunit of non-bifurcating NADH-dependent [FeFe]-hydrogenases differs from those of multimeric electron-bifurcating [FeFe]-hydrogenases. *Front. Microbiol.* **11**, 1109 (2020).
33. J. Zivanov, T. Nakane, B. O. Forsberg, D. Kimanius, W. J. H. Hagen, E. Lindahl, S. H. W. Scheres, New tools for automated high-resolution cryo-EM structure determination in RELION-3. *Elife.* **7**, e42166 (2018).
34. A. Rohou, N. Grigorieff, CTFFIND4: Fast and accurate defocus estimation from electron micrographs. *J. Struct. Biol.* **192**, 216–221 (2015).
35. J. Zivanov, T. Nakane, S. H. W. Scheres, Estimation of high-order aberrations and anisotropic magnification from cryo-EM data sets in RELION-3.1. *IUCrJ.* **7**, 253–267 (2020).
36. N. W. Moriarty, P. D. Adams, Iron–sulfur clusters have no right angles. *Acta Crystallogr. Sect. D Struct. Biol.* **75**, 16–20 (2019).

37. M. Nouailler, X. Morelli, O. Bornet, B. Chetrit, Z. Dermoun, F. Guerlesquin, Solution structure of HndAc: A thioredoxin-like domain involved in the NADP-reducing hydrogenase complex. *Protein Sci.* **15**, 1369–1378 (2006).
38. L. A. Kelley, S. Mezulis, C. M. Yates, M. N. Wass, M. J. E. Sternberg, The Phyre2 web portal for protein modeling, prediction and analysis. *Nat. Protoc.* **10**, 845–858 (2015).

Declarations

Acknowledgments

This work benefited from access to the Astbury Biostructure Laboratory, an Instruct-ERIC centre. Financial support was provided by Instruct-ERIC (PID 11666). We are grateful to Svetomir Tzokov, Charlotte Scarff, and Rebecca Thompson for assistance with data collection and Nigel Moriarty for assistance with FeS ligation during model building. We used computational resources provided by the Viking Cluster at the University of York and are grateful to the Research Computing team and Huw Jenkins for assistance with computing. We thank Mikroanalytisches Laboratorium Kolbe for ICP-MS measurements. We are grateful to Hannah Bridges, Laure Decamps and Patrícia Rodríguez Maciá for critical evaluation of the manuscript. J.A.B. and N.C. acknowledge funding from the DFG SPP 1927 “Iron–Sulfur for Life” project (Project No. BI 2198/1-1). The work was supported by the Max Planck Society (J.A.B., N.C. and W.L.), and in part a UKRI Future Leader Fellowship (JNB; MR/T040742/1) and JSPS KAKENHI (Grant number 16K21748 (H.O.).

Author contributions

Conceptualization: NC, HO, WL, JNB, JAB

Methodology: CF, NC, PG, JNB, JAB

Investigation: CF, NC, PG, JNB, JAB

Visualization: CF, PG, JNB

Funding acquisition: JNB, JAB

Project administration: JAB, JNB

Supervision: JAB, JNB

Writing – original draft: CF, NC, JNB, JAB

Writing – review & editing: CF, NC, PG, HO, WL, JNB, JAB

Competing interests

Authors declare that they have no competing interests.

Data and materials availability

Protein databank (PDB) files for the four model presented in this manuscript are available at https://www.rcsb.org/ under PDB ID 7P5H (D2 tetramer, 7P8N (Bridge closed forward), 7P91 (Bridge closed reverse), and 7P92 (Open bridge). Cryo-EM maps are available at https://www.ebi.ac.uk/pdbe/emdb/. All other data are available in the main text or the supplementary materials.

Figures

Figure 1

(A) The unsharpened 2.3 Å map of Hyd(ABC)4 with D2 symmetry enforced showing a tetramer of HydABC heterotrimers. All four copies of HydB and C are colored blue and green, respectively. The four HydA copies that make up the core of the complex are in orange, yellow, pink, and red. The top and bottom halves of the complex are constituted by dimers of HydABC protomers (each HydABC unit is a protomer); the two protomers within the same dimer are strongly interacting, while a weaker interaction is present between the top and bottom dimers. (B) HydABC dimer highlighting the iron-sulfur clusters and FMN constituting the electron transport network. (C) The arrangement of redox cofactors within the protein complex, showing two independent identical redox networks (dashed circles); each redox network is composed of iron-sulfur clusters belonging to a Hyd(ABC)2 unit composed of two strongly interacting HydABC protomers. (D) Schematic of the electron transfer network of one of the two identical Hyd(ABC)2 units showing edge-to-edge distances (in Å) between the various cofactors.

Figure 2

(A) Subunits HydA (red), HydB (blues) and HydC (green) overlaid with, respectively, Nqo3, Nqo1, Nqo2 (all yellow) of complex I from T. thermophilus (PDB 6ZIY) (13). (B) Comparison of the NADH binding site of the Nqo1 subunit of complex I from Thermus Thermophilus (light blue) with the FMN site in HydB; the high similarity suggests NADH binds in the proximity of FMN in HydABC similarly to complex I. (C) Electron transfer network in HydABC compared to complex I from T. thermophilus.

Figure 3

(A) HydA from Thermotoga maritima (red) compared with CpI hydrogenase from Clostridium pasteurianum (orange) (PDB: 4XDC) (29). (B) Electron transfer network in HydA showing the iron-sulfur

cluster that electrically connects adjacent HydABC protomers (red circle). (C) Electron transfer network in CpI , with Cp ferredoxin, predicted to bind closely to the iron-sulfur cluster on the right (28). Note that only the [4Fe-4S]H subcluster of the H-cluster is present in our TmHydA structure, whereas the complete H-cluster including the [2Fe]H subcluster is present in the CpI structure.

Figure 4

(A) The unsharpened 2.8 Å map of the bridge forward class sub-particle, identical to the bridge backward class if a C2 rotation is applied. The map shows only the Hyd(ABC)2 unit as the two Hyd(ABC)2 units constituting the Hyd(ABC)4 complex were found to be independent after 3D classification. All four copies of HydB and C are colored blue and green, respectively. The two HydA copies are in light brown and light red. (B) Local resolutions were estimated using the local resolution function in RELION with default parameters. (C) The atomic model that was built into the map density with the iron-sulfur electron transfer chain. (D) Map showing the HydB bridge domain in the open position and its fitted model. (E) Zn2+ hinge region, showing the two possible conformations of the HydB bridge domain, open (blue) and closed (light blue). (F) Schematic of the electron transfer network of one of the two identical Hyd(ABC)2 units showing edge-to-edge distances (Å) between the components. Represented are the iron-sulfur clusters, H-cluster, FMN and Zn2+ site; the bridge components and Zn-site are enclosed in a dashed ellipse. Each of the two HydABC protomers constituting the Hyd(ABC)2 unit is included within a dashed rectangle. Here the top bridge is represented in its closed conformation, while the bottom one is in its open conformation.

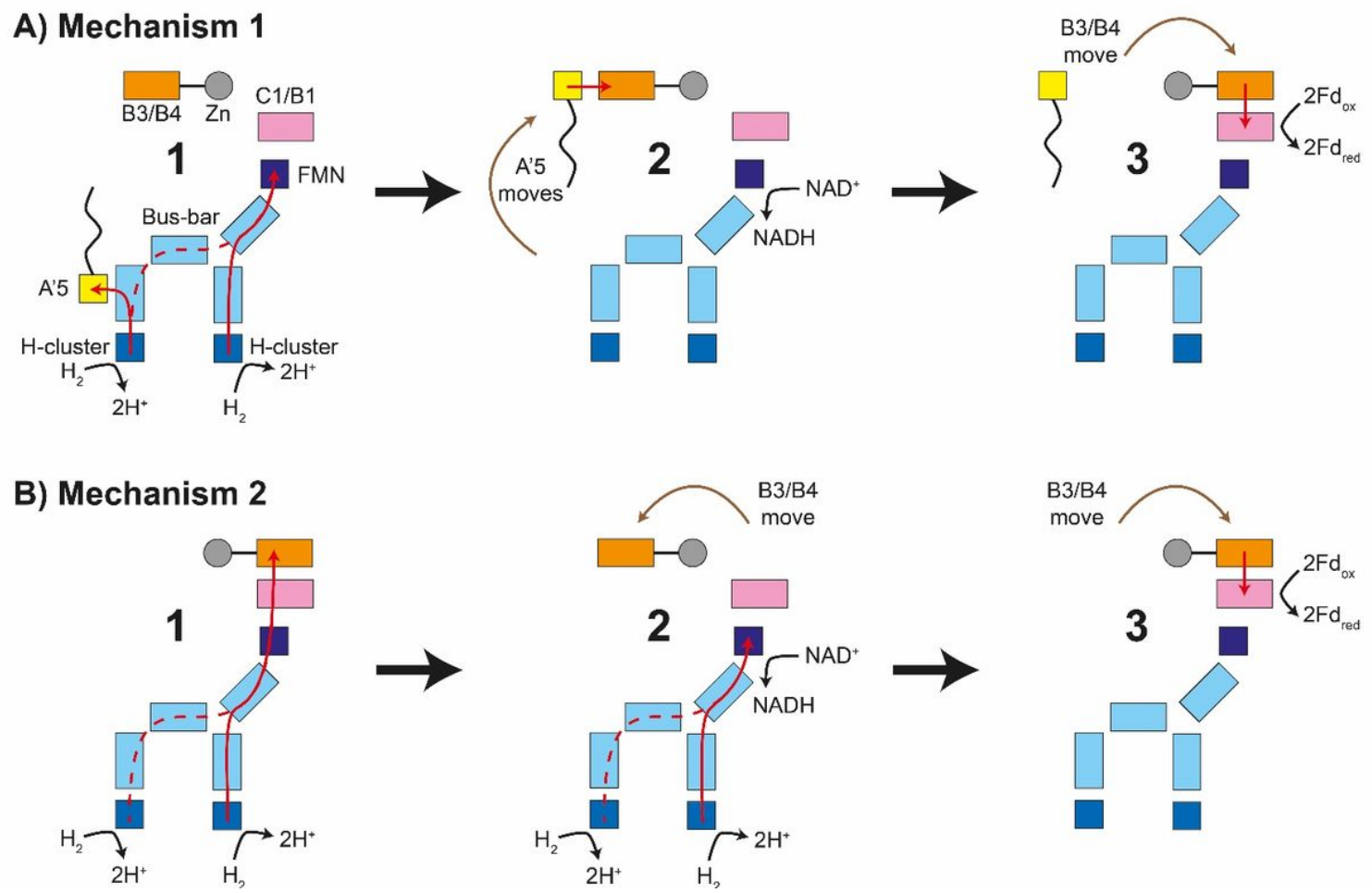

Figure 5

Illustration of two possible mechanisms of electron transfer in HydABC. A) In Mechanism 1, electrons from H2 oxidation at the H-cluster are transferred to the FMN, via the core electron transfer pathway and cluster A´5 (step 1). A large conformational change moves A´5 close to the B3/B4 cluster pair in the bridge allowing electron transfer (step 2). This needs to occur twice to put two electrons in the B3/B4 pair. At the same time, NAD+ binding and hydride transfer at the FMN forms NADH, triggering a conformational change in the bridge, moving the B3/B4 clusters close enough to the B1/C1 clusters for electron transfer (step 3). Ferredoxin can then accept the electrons from B1. B) In Mechanism 2, electrons generated by oxidation of H2 at the H-cluster travel down the core electron transfer pathway to the FMN and C1 cluster, and then to the B3/B4 cluster pair (step 1) closing the bridge (step 2). Further H2 oxidation reduces the FMN leading to NAD+ reduction to NADH. This triggers bridge movement allowing the B3/B4 clusters to transfer electrons to the B1/C1 clusters and then to ferredoxin. Red arrows indicate electron transfer, brown arrows indicate domain movement, and black arrows indicate a catalytic step. Color code: dark blue squares (H-cluster), light blue rectangles (core electron transfer pathway), purple square (FMN), pink rectangle (electron transfer pathway to ferredoxin), orange rectangle (bridge domain electron transfer pathway), gray circle (Zn site), yellow square (cluster A´5).

Supplementary Files

This is a list of supplementary files associated with this preprint. Click to download.

- Furlan2021NSMBSI23Nov2021.docx
- MovieS1.mp4
- MovieS2.mov